Multiscale study of the influence of chemical order on the properties of liquid Li-Bi alloys

J.-F. Wax
Laboratoire de Physique des Milieux Denses, Université Paul Verlaine - Metz, 1, Boulevard F. D. Arago, F-57078 Metz Cedex 3, France

M. R. Johnson
Institut Laue Langevin, 6 rue Jules Horowitz, F-38042 Grenoble Cedex 9, France

L. E. Bove
Physique des Milieux Denses, IMPMC, CNRS-UMR 7590, Université Pierre et Marie Curie, F-75252 Paris, France

M. Mihalkovič
Institute of Physics, Slovak Academy of Sciences, Dubravska cesta 9, 84511 Bratislava, Slovakia
(Received 22 July 2010; revised manuscript received 22 November 2010; published 13 April 2011)

The static structure and diffusion properties of Li-Bi liquid alloys at three compositions are investigated by molecular dynamics simulations. Due to the strong chemical order shown by these alloys, a multiscale approach is applied, fitting empirical pair potentials to data from *ab initio* molecular dynamics simulations to subsequently perform large-scale classical simulations. In this way, the partial structure factors as well as the self-diffusion and interdiffusion coefficients can be computed with sufficient accuracy to be discussed quantitatively. This approach is validated by comparing our predictions with experimental structure factor measurements. A marked heterocoordination is observed, which strongly influences the diffusion properties. These observations are consistent with an evolution toward ionic bonding at the Li_{75}-Bi_{25} composition.

DOI: 10.1103/PhysRevB.83.144203 PACS number(s): 61.25.Mv, 61.20.Ja, 66.10.cg, 34.20.Cf

I. INTRODUCTION

When computing the static and dynamic structure of a liquid alloy by molecular dynamics (MD) simulation, two conditions have to be fulfilled. The first one is to accurately describe the interactions between the atoms inside the liquid and the second one to consider a box large enough over a time long enough to ensure good statistics and sufficient resolution into space and time.

Ab initio MD (AIMD) fully meets the first condition but often struggles with the second one, while classical MD (CMD) using pair potentials is faced with the opposite dilemma. Consequently, accurately simulating physical properties of a liquid alloy is not a trivial task. The fact is that, for the most part, the alloys for which an accurate description of the interactions in terms of pair potentials is available are rather simple mixtures with no strong chemical order.[1,2] However marked homocoordination or heterocoordination tendencies strongly affect the physical properties of a mixture, making such systems more appealing.

Therefore, it is interesting to setup a methodology giving an accurate description of the interactions in terms of empirical pair potentials working for such complicated systems. We have applied a force-matching technique in the same spirit as the pioneering work of Ercolessi and Adams,[3] but adapted by Mihalkovič *et al*.[4] to obtain efficient pair potentials in the case of metallic alloys. Starting from AIMD performed with the VASP code,[5,6] three analytic partial pair potentials are fitted to reproduce the *ab initio* computed forces and energy differences in the liquid under given thermodynamic conditions. These pair potentials are then introduced in a CMD simulation to increase the size of the simulated system. Considering first the static structure, it is possible to reach q values low enough to get clear insight about chemical order. Moreover, being able to run simulations over longer times, self-diffusion and interdiffusion properties (and more generally, dynamic properties) can also be investigated.

We have chosen to apply this multiscale approach to the Li-Bi system for the following reasons. First, there is a strong difference between the valencies of both components, which presumably will induce marked heterocoordination tendencies. The electronegativity difference between both species may induce some ionic nature to the bonding between Li and Bi atoms in this mixture. Indeed, the electronic transport properties, which we will discuss in more detail later, indicate a strong departure from a simple metallic behavior. Considering the phase diagram,[7] we can point out the congruently melting intermetallic compound, Li_3-Bi, which is likely to have repercussions in the liquid phase.[8] Second, Li_{30}-Bi_{70} has been studied recently by inelastic neutron scattering[9] and it has been shown that the high mass ratio ($M_{Bi}/M_{Li} = 30.1$) is responsible for the peculiar behavior of the collective excitations. This is likely also to be the case for the diffusion properties. To examine the influence of the composition of the mixture, we have considered three compositions, namely Li_{30}-Bi_{70}, Li_{57}-Bi_{43}, and Li_{70}-Bi_{30}; the extreme compositions have been the subject of experimental investigations that are partially published[9] while the intermediate has still to be measured. From the aforementioned measurements, an estimation of the static structure factor can be derived. This will enable us to check the validity of the description of the interactions by comparing the simulation and experimental results. Thus Li-Bi alloys constitute an interesting benchmark for our approach for which we have computed both the static structure and the diffusion properties.

This paper is organized as follows. After this Introduction, the next section will gather all the useful technical details.

Then, in Sec. III, we will display our results which will be analyzed following two lines, the first one being the check of the accuracy of the approach and the second one being the study of several properties of these nonsimple mixtures, namely their electronic and static atomic structures as well as their diffusion properties. Finally, the main conclusions will be summarized in Sec. IV which will end with an overview of possible, future applications of this approach.

II. FORMALISM AND SIMULATION DETAILS

A. *Ab initio* simulations and density determination

We have considered three compositions, namely Li_{30}-Bi_{70}, Li_{57}-Bi_{43}, and Li_{70}-Bi_{30}. There is one important thermodynamic datum to be considered when dealing with metallic systems, namely the density since it is well established that interatomic interactions in these systems are strongly density dependent. For alloys however, experimental values are often lacking in the literature and this is the case of the Li-Bi ones. Indeed, to our knowledge, density data are available only for compositions between 4 and 26.8 at % Bi.[10]

We could have estimated the density as a function of composition by linearly interpolating between the pure liquid values, but since we were suspecting strong heterocoordination tendencies, this seemed to be too crude an approximation. In addition, a reduction of the volume by about 30% is observed at the Li_{75}-Bi_{25} composition, which was interpreted as a consequence of ionic-like bonding. Therefore, we proceeded in the following way to estimate it more realistically at each composition and temperature. We performed AIMD simulations at several densities and computed the pressure in each state allowing the equilibrium density to be determined by interpolation. These simulations were performed using 50 particles in the canonical ensemble (constant N, V, and T). The time step was 3 fs (we checked that results were not different using a 1 fs time step) and the runs were typically 1000 steps long, a duration sufficient to reach equilibrium. Due to the small size of the simulated systems, fluctuations of pressure were rather important, but this approach nevertheless allowed a reliable estimate of the density.

Electronic and ionic first-principles calculations were carried out using the projector-augmented wave (PAW) formalism[11] of the Kohn-Sham density functional theory (DFT)[12,13] at the generalized gradient approximation level (GGA), implemented in VASP . The GGA was formulated by the Perdew-Burke-Ernzerhof (PBE)[14,15] density functional. A single k point (the gamma point) was used in the electronic structure determination.

The density values obtained are gathered in Table I. They are quite different from those provided by a linear interpolation between the values of the pure metals (9.38 and 0.45 g/cm^3 for Bi and Li at 1073 K, respectively). We stress that this is only a way to estimate the density in view of the lack of experimental data. Moreover, as shown in Fig. 1, they agree with the scarce, available experimental data.

B. Determination of the interaction potentials

Interactions are accurately described in AIMD simulations since the electronic structure is computed from first principles.

TABLE I. Temperatures and densities at which the three systems were studied.

System	Density (g/cm^{-3})	T (K)
Li_{30}-Bi_{70}	8.28	673
Li_{57}-Bi_{43}	6.45	1073
Li_{70}-Bi_{30}	4.73	1073

Therefore, such runs can be considered as reference data that one may try to mimic by simpler analytical expressions.

In our approach, the first step consisted of performing AIMD simulations under the desired thermodynamic conditions and compositions. These runs were performed using the VASP code. The box contained 200 particles and was sized to reproduce the desired density (Table I). The setup of the simulation was mentioned above except that they lasted 10 000 time steps. These simulations were used to get the electronic density of states for each system, as well as the partial pair distribution functions $g_{ij}(r)$, which will be presented in Sec. III.

Our three pair potentials $u_{ij}(r)$ were fitted to the six-parameters form of Ref. 4, namely

$$u_{ij}(r) = \frac{C_{ij}^{(1)}}{r^{\eta_{ij}^{(1)}}} + \frac{C_{ij}^{(2)}}{r^{\eta_{ij}^{(2)}}} \cos(k_{ij} r + \phi_{ij}). \quad (1)$$

This form has a repulsive core (first term in the equation involving parameters $C_{ij}^{(1)}$ and $\eta_{ij}^{(1)}$) and an oscillating tail (second term involving parameters $C_{ij}^{(2)}$, $\eta_{ij}^{(2)}$, k_{ij}, and ϕ_{ij}). While this expression has been designed for simple-metal rich mixtures with transition metals, the interplay between the repulsive part and the oscillating tail provides for flexibility and efficiency in parametrization, which prove appropriate in many other situations. In the Li-rich case, for instance, the oscillating tail turned out to be redundant for Li-Li interactions and they were fitted using a repulsive shell only (two parameters).

For each of the three compositions of interest, we fitted the parameters of the potentials to reproduce both the forces and

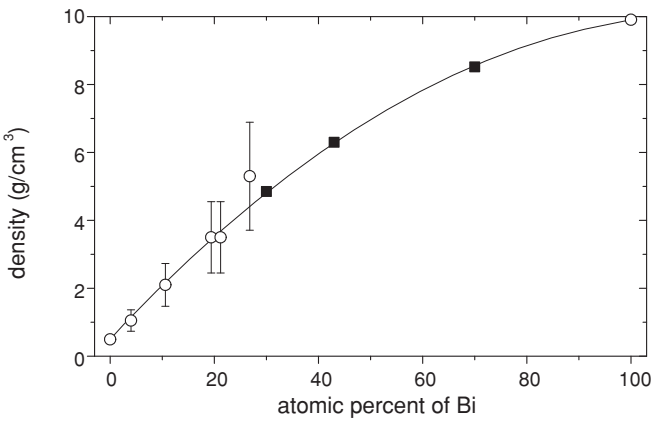

FIG. 1. Density of liquid Li-Bi alloys as a function of composition. Full squares are predictions of NPT *ab initio* simulations while open circles are experimental data from Ref. 10. The line is a guide for the eyes interpolating between pure elements and simulation values.

TABLE II. Features of the fitting procedure for each composition (see text).

Composition	Forces	Energy diff.	rms(F) [eV/Å]	rms(E) meV/atom	Samples at T[K]
Li_{70}-Bi_{30}	7812	9	0.145	2.6	300; 600; 900; 1500
Li_{57}-Bi_{43}	7830	17	0.151	3.9	300; 600; 900; 1500
Li_{30}-Bi_{70}	2400	3	0.165	0.4	1500

the energy differences for the 200 atom configurations from the VASP simulations. More precisely, the parameters were fitted to reproduce the forces undergone by each particle in several selected snapshots. Since fits from forces alone are insufficiently constrained, we also required energy differences to be reproduced to improve them. The energy differences are defined as the variation of the total energy between a low temperature system and a high temperature one, both with the desired composition and density. The low temperature references considered here were always $T = 300$ K.

Details about the fitting procedure are summarized in Table II where columns "forces" (force components for all atoms in all samples) and "energy diff." specify the number of data points considered for each quantity. The columns "rms" denote r.m.s. deviations of the respective fit, and the column "samples" lists the temperatures at which snapshots were taken to determine energy differences. The overall efficiency is illustrated in Fig. 2 where *ab initio* and fitted forces are plotted for each considered configuration.

The parameters are gathered in Table III, and readers are referred to Ref. 4 for further details about the fitting procedure.

C. Large-scale classical simulations

Once the fitted pair potentials are known, CMD simulations can be performed to investigate more accurately the static structure as well as the diffusion properties. Among them, interdiffusion, which is a collective dynamic property

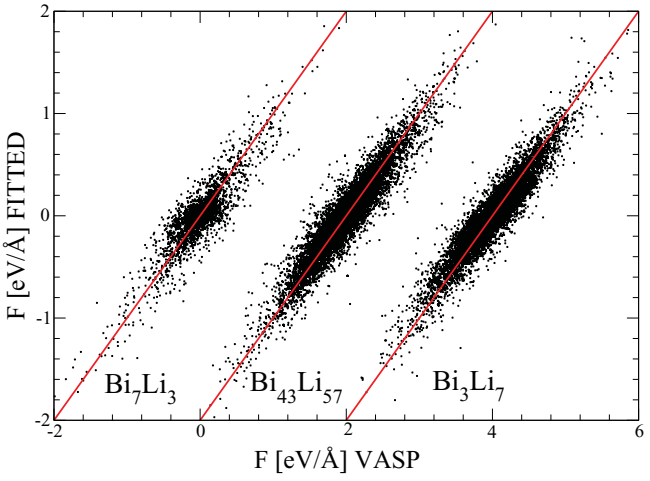

FIG. 2. (Color online) Fitted forces versus *ab initio* ones for each configuration considered. Data corresponding to Li_{57}-Bi_{43} and Li_{30}-Bi_{70} are shifted by 2 and 4 eV/Å along the horizontal axis, respectively.

definitely beyond the scope of AIMD. So, in the spirit of recent work on liquid Na-K and K-Cs mixtures, we launched two different kinds of NVE classical simulations for each composition.

The first one, involving 13 500 atoms over 100 000 time steps, allowed us to get $g_{ij}(r)$ over a wide spatial range, leading to the low-q behavior of the static structure factors down to q less than about 0.1 Å^{-1}. The second one with 2048 particles during 5 000 000 time steps was used to compute the self-diffusion and interdiffusion properties. Due to the very light mass of lithium atoms, the time step was chosen as low as 0.1 fs to ensure the stability of the temperature during the NVE simulations. Thus, the observed temperature drift along the 500 ps simulations was less than 0.5%.

As we shall see in Sec. III, the accuracy of these simulations was ascertained by comparing their predictions with available experimental and *ab initio* results. Further details concerning both the classical simulations and the computation of the physical properties of interest can be found in Refs. 1 and 2.

D. Experimental data

The measurement of the static structure factor $S(q)$ of a liquid as a function of the wave vector q is usually performed with elastic x rays or neutrons scattering experiments. However, it can also be determined from inelastic scattering provided a large-enough frequency range is available. Indeed,

$$S(q) = \int_{-\infty}^{+\infty} S(q,\omega)\, d\omega, \tag{2}$$

where $S(q,\omega)$ is the dynamic structure factor. Thus, we took advantage of the existence of such experimental inelastic data, performed to investigate collective excitations in liquid Li-Bi alloys to evaluate $S(q)$.

The experimental quantities reported in this article are the energy-integrated dynamic structure factor for Li_{70}-Bi_{30}, and the total scattering factor as measured directly on the detector (i.e., without energy discrimination) for Li_{30}-Bi_{70}. In the first case, the quantity has been deduced from the measured dynamic structure factor. In the second case, the total scattering factor has been directly measured during the experiment campaign as a test for melting, but the data were not reported in Ref. 9.

For greater convenience, we recall a few characteristics of these experiments and interested readers are requested to refer to Refs. 9 and 18 for further details. Inelastic neutron scattering measurements were carried out at the three-axis spectrometer IN1 of the Institut Laue-Langevin (ILL, Grenoble, France). The Li_{30}-Bi_{70} and Li_{70}-Bi_{30} metal alloys were prepared by melting high purity Li (99.99%) and Bi (99.99%) at 673

and 1073 K, respectively, until complete mixing of both components. The intensity scattered by the sample was then measured at several wave vector transfer values, between $q = 0.5$ and 2 Å^{-1} for Li_{70}-Bi_{30} and up to 2.5 Å^{-1} for Li_{30}-Bi_{70}. The so-derived dynamic structure factors showed two distinct doublets peaked at different frequencies. The presence of two well-defined coexisting modes showing an optic- and acoustic-like behavior, respectively, is in line with the heterocoordinated nature of the alloy.

The measured dynamic structure factors were then integrated over an extended energy range to obtain an estimation of the total static structure factor to be compared with the present simulations. Since these inelastic scattering experiments were performed separately for Li_{30}-Bi_{70}[9] and Li_{70}-Bi_{30}, the quality of the experimental determination of $S(q)$ was not the same. We will come back to this point when considering the results.

III. RESULTS

A. Electronic structure

The first physical property we discuss is the electronic density of states. The *ab initio* computed results are displayed in Fig. 3. As can be seen, valence electrons split into two bands. This was also observed in pure liquid bismuth both experimentally[16] and theoretically.[17] Considering the computed number of electronic states, the lowest energy band is filled with the two 6*s* electrons of bismuth atoms, while the highest energy one is filled with both the three 6*p* electrons of bismuth and the single 2*s* electron of lithium.

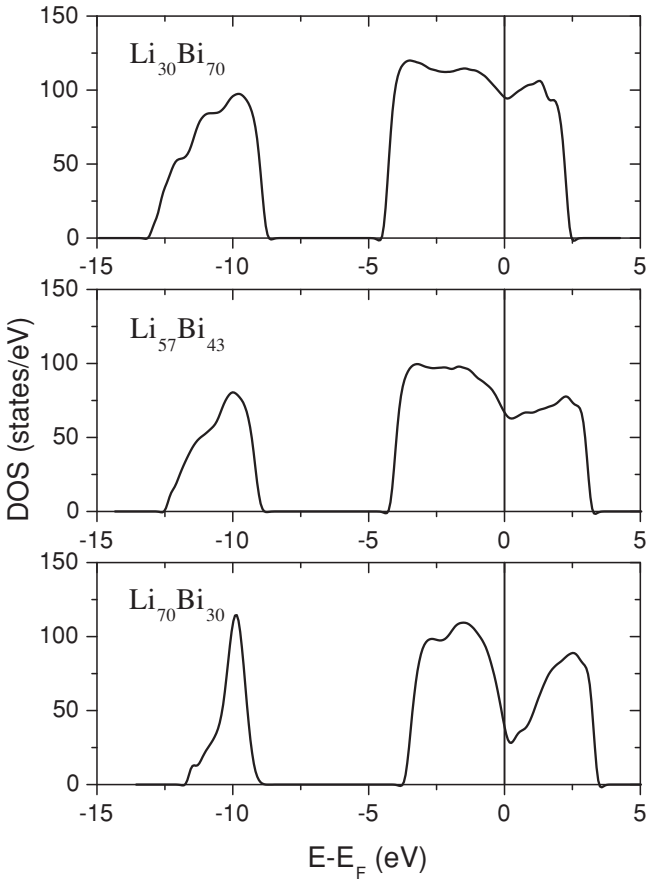

FIG. 3. Electronic density of states for each alloy under consideration as obtained from *ab initio* simulations.

The energy gap between both bands is quite high (about 5 eV) and prevents any transition of electrons from the 6*s* band to the Fermi level. Moreover, at the Fermi energy, a pseudogap appears that deepens as the bismuth concentration decreases. Consequently, the metallic character of the alloy becomes impaired when going from 30 to 70 at. % of lithium. Since liquid lithium is a good electrical conductor, we can predict a reversal of this trend between 70 and 100 at. % of Li.

This evolution versus composition is confirmed by electrical resistivity measurements.[10] While liquid Li and Bi are metallic at melting with respective electrical resistivities of about 25 and 130 $\mu\Omega$/cm and positive temperature coefficients, the observed value at the stoichiometric composition Li_3Bi grows up to 2000 $\mu\Omega$/cm and the temperature coefficient becomes negative. This unambiguously indicates a loss of the metallic nature of the electronic structure and a strengthening of the ionic character, which is corroborated by spin relaxation[19] and magnetic susceptibility[20] measurements. It also is consistent with the phase diagram of the alloy[7] exhibiting a congruently melting Li_3Bi intermetallic compound. We will come back to this point later when considering the other physical properties of interest.

B. Pair potentials

This nonsimple electronic structure, far from nearlyfree-electron-like, prevents a self-consistent screening formalism from being applied to obtain effective pair potentials from the second-order perturbation method, as is possible in simple metals like liquid lithium, for instance. Indeed, the density of states (DOS) is too different from a parabolic one, so that these alloys cannot be considered as simple metals. The use of empirical pair potentials is justified in this way. As mentioned above, we have fitted potentials from *ab initio* VASP simulations using expression (1). The values of the parameters are displayed in Table III and the corresponding curves are shown in Fig. 4, which reveal some interesting features.

The repulsion range of $u_{\mathrm{BiBi}}(r)$ is longer than that of $u_{\mathrm{LiLi}}(r)$, and it exceeds the ratio of the corresponding ionic core radius. As a consequence, whatever the composition, bismuth atoms will repel each other in such a way that a lithium atom will easily intercalate in between. The interactions are not additive in the sense that $u_{\mathrm{LiBi}}(r)$ is not the mean of the other two, especially concerning the repulsion. In addition, when increasing the lithium concentration, it clearly appears that lithium-bismuth attraction becomes preponderant. It is also interesting to point out that the lithium-lithium interaction, as fitted by our method in the case of Li_{70}-Bi_{30}, is purely repulsive. Even if the value of $\eta_{12}^{(1)}$ does not correspond to a Coulombic interaction, this trend has to be related to the above-mentioned evolution toward an ionic character of the interactions in this range of composition.

TABLE III. Values of the parameters of the pair potentials. Units are such that distances are in Å and energies in eV.

System	$i-j$	$C_{ij}^{(1)}$	$\eta_{ij}^{(1)}$	$C_{ij}^{(2)}$	$\eta_{ij}^{(2)}$	k_{ij}	ϕ_{ij}
	Li-Li	509.05117	8.72399	19.65249	5.90901	3.26752	4.07121
Li_{30}-Bi_{70}	Li-Bi	54.45000	5.88803	−149.35784	7.18473	2.47563	4.04811
	Li-Li	452.88095	6.02955	−42.98817	5.30268	3.41151	2.01862
	Li-Li	968.07392	10.44178	33.66214	6.35754	3.07433	4.97542
Li_{57}-Bi_{43}	Li-Bi	56.90363	6.26837	−85.04891	6.43670	2.52266	4.36167
	Bi-Bi	173.12510	5.08537	−183.41762	6.16428	3.02983	3.10465
	Li-Li	396.02798	8.73571	0.00000	0.00000	0.00000	0.00000
Li_{70}-Bi_{30}	Li-Bi	2612.40127	12.46890	−55.12306	5.44045	2.20358	5.53860
	Bi-Bi	2080.53828	7.28471	−58.80280	4.67069	2.53289	5.26020

Of course, these fitted pair potentials have to be checked by comparing their predictions to experimental or *ab initio* data to validate the fitting procedure.

C. Static structure

The static structure results are used in two ways, first to check the reliability of the fitted pair potentials and second to investigate the atomic order in the alloys.

1. Check of the potentials

We first consider the VASP simulations used to fit the pair potentials as reference data. We thus discuss the agreement between classical and *ab initio* simulations. The partial pair distribution functions of each alloy obtained in both ways are presented in Fig. 5.

For each composition, the partial structure functions $g_{ij}(r)$ are qualitatively well reproduced. Peak positions coincide, so

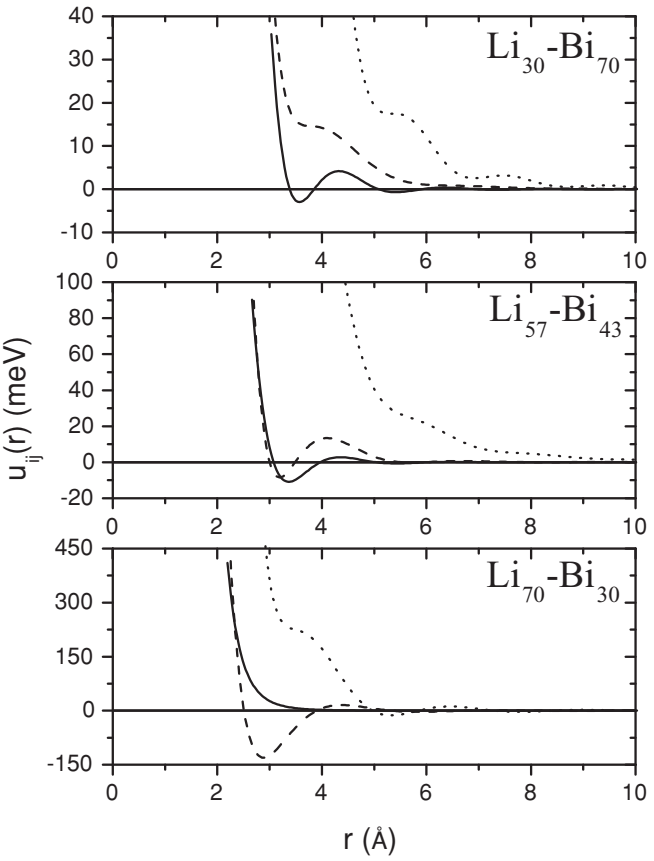

FIG. 4. Pair potentials fitted from *ab initio* MD simulations and used to mimic the behavior of the systems in the classical simulations performed in this study (Li-Li: solid; Li-Bi: dashed; Bi-Bi: dotted).

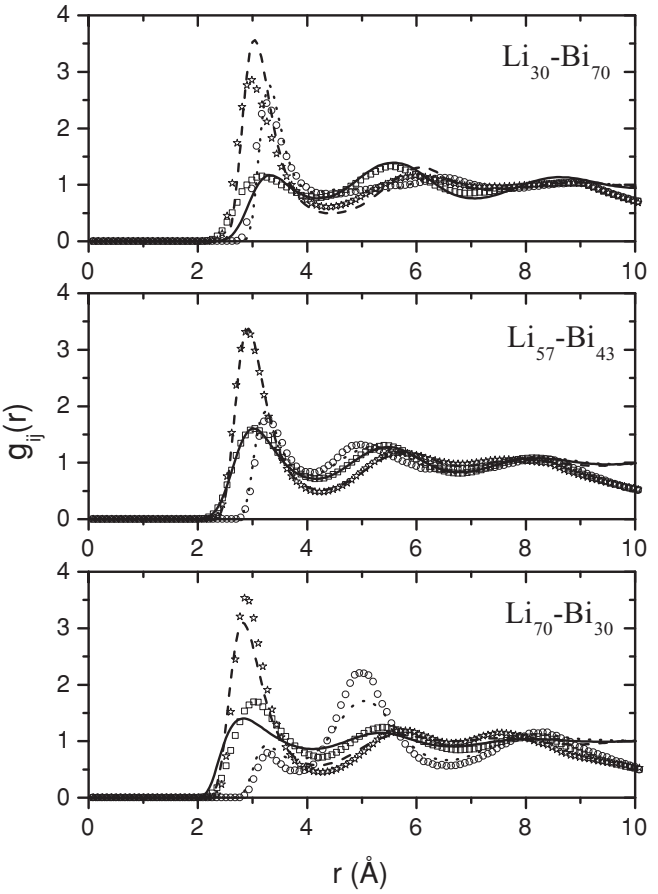

FIG. 5. Partial pair distribution functions obtained for the three alloys under consideration. Symbols are used for *ab initio* results (Li-Li: squares; Li-Bi: stars; Bi-Bi: circles) and lines correspond to classical simulations (Li-Li: solid; Li-Bi: dashed; Bi-Bi: dotted).

the topological order is recovered. The hierarchy between the peak heights is also obeyed and so is the chemical order. There is not a quantitative agreement between the intensities of the peaks, except in the case of Li_{57}-Bi_{43} for which a remarkably good agreement is observed. Nevertheless, according to the extremely peculiar structure of these mixtures, which we will discuss later, we consider that the way such simple pair potentials (with no many-body effects) succeed in mimicking the structure of the alloys is adequate.

We now discuss the realism of the interactions by considering the experimental results. Although the number of atoms was quite high for an AIMD simulation, it was not sufficient to compute the partial structure functions over a range large enough to allow the Fourier transform to be performed accurately to get the Ashcroft-Langreth partial structure factors[21] defined as

$$S_{ij}(q) = \delta_{ij} + \sqrt{c_i c_j}\rho \int_0^\infty [g_{ij}(r) - 1]\frac{\sin qr}{qr} 4\pi r^2 dr, \qquad (3)$$

where c_i is the concentration of the ith species and $\rho = N/V$ is the number density. This was also true if one tried to compute it straight from the configurations using

$$S_{ij}(q) = \frac{1}{\sqrt{N_i N_j}} \left\langle \sum_{b=1}^{N_i} \sum_{a=1}^{N_j} \exp(i\vec{q} \cdot \vec{R}_{ab}) \right\rangle, \qquad (4)$$

because the simulated time was not long enough to reasonably lower the statistical noise. So the only calculated structure factors that we can consider stem from the CMD simulations of larger boxes performed using the fitted potentials.

We recombined the partial structure factors (which will be discussed later) to evaluate the total structure factors as measured in neutron diffusion experiments

$$S(q) = \frac{c_1 b_1^2 S_{11}(q) + 2\sqrt{c_1 c_2} b_1 b_2 S_{12}(q) + c_2 b_2^2 S_{22}(q)}{c_1 b_1^2 + c_2 b_2^2}, \qquad (5)$$

with b_i corresponding to the coherent diffusion length describing the diffusion of an incident neutron by an atom of type i ($b_{\mathrm{Li}} = -1.90$ fm and $b_{\mathrm{Bi}} = 8.532$ fm). Interestingly, the total $S(q)$ obtained with neutrons are rather distorted, which can be interpreted as a signature of an underlying order. As can be observed in Fig. 6, the total structure is very sensitive to the composition: the position of the first peak shifts to higher q values as c_{Bi} increases and its height simultaneously decreases. This is qualitatively recovered in the simulation data which moreover display minor second peaks or shoulders in the first one.

While the agreement with the experimental data is excellent for Li_{70}-Bi_{30}, this is not the case for the Bi-rich composition. As we explained in Sec. II, the experimental data were not obtained from the same experiment campaign. In the early case of the Bi-rich alloy, inelastic data were not collected with the intention to deduce the total structure factor and the data reported here have been obtained from a melting-check scan, performed removing the three-axis analyser, to collect directly the full scattered intensity on the detector. In such a way, we used the three-axis spectrometer as a two-axis diffractometer, with no energy analysis. Anyway, neither detector efficiency correction nor multiple scattering corrections have been performed on the raw data. Therefore,

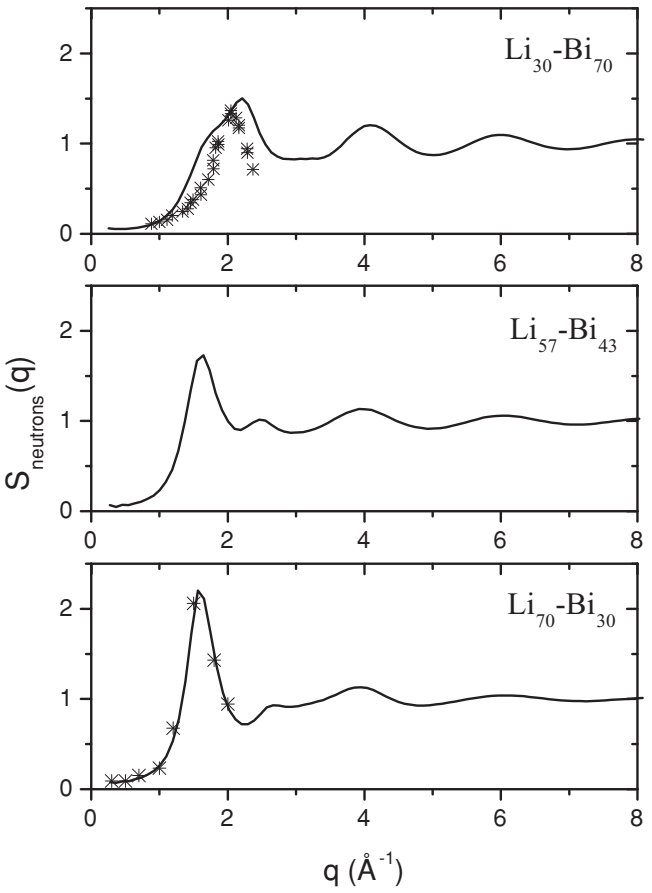

FIG. 6. Total structure factors for neutrons (full line: simulation; symbols: experiment).

we believe that these early results are rather of qualitative than quantitative value. Conversely, the Li-rich composition data have been collected and analyzed following the rigorous procedure described in Sec. II and are thus more reliable. Nevertheless, the overall evolution is recovered and the agreement with the reliable experimental data is good, which validates our whole approach.

Finally, the fitted pair potentials are well suited to reproduce, at least qualitatively, the microscopic behavior of this alloy. Indeed, their predictions are in agreement with both experimental and AIMD simulation results. This statement allows us to investigate now in more detail the static structure.

2. *Static structure analysis*

Let us first consider the VASP results (Fig. 5). The partial structures are very different from those observed in nearly random alloys like K-Cs (Ref. 1) or Na-K (Ref. 2). At each composition under study, the alloy exhibits a strong heterocoordination as indicated by the first peak of the cross-function $g_{\mathrm{LiBi}}(r)$ which is higher than the corresponding peaks of the two other functions. Among these alloys, Li_{57}-Bi_{43} shows the usual hierarchy between the successive peaks of each partial function. But, in both others, the first peak of the

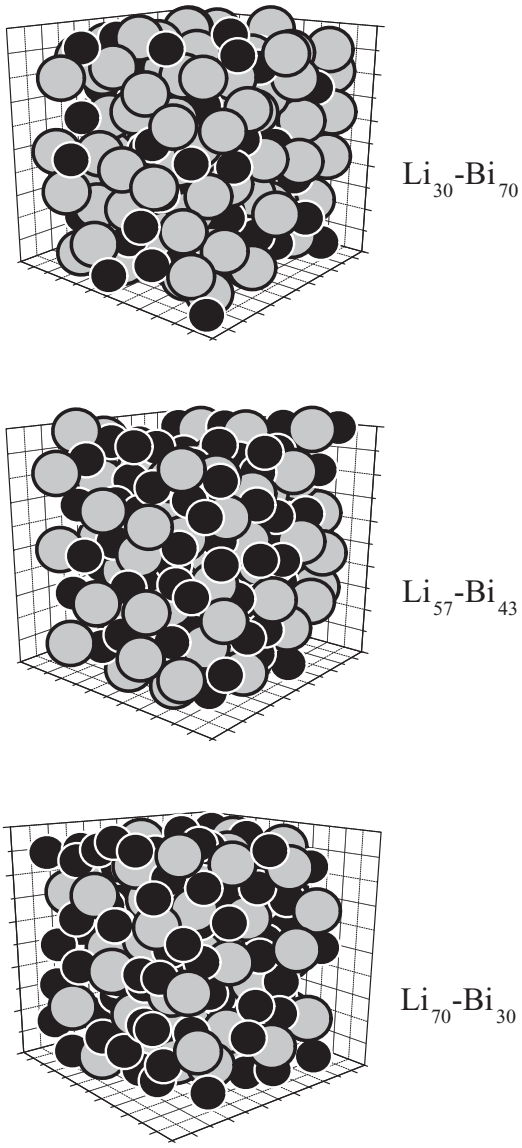

FIG. 7. Snapshot of the simulation boxes in AIMD simulations (Li: black circles; Bi: grey circles).

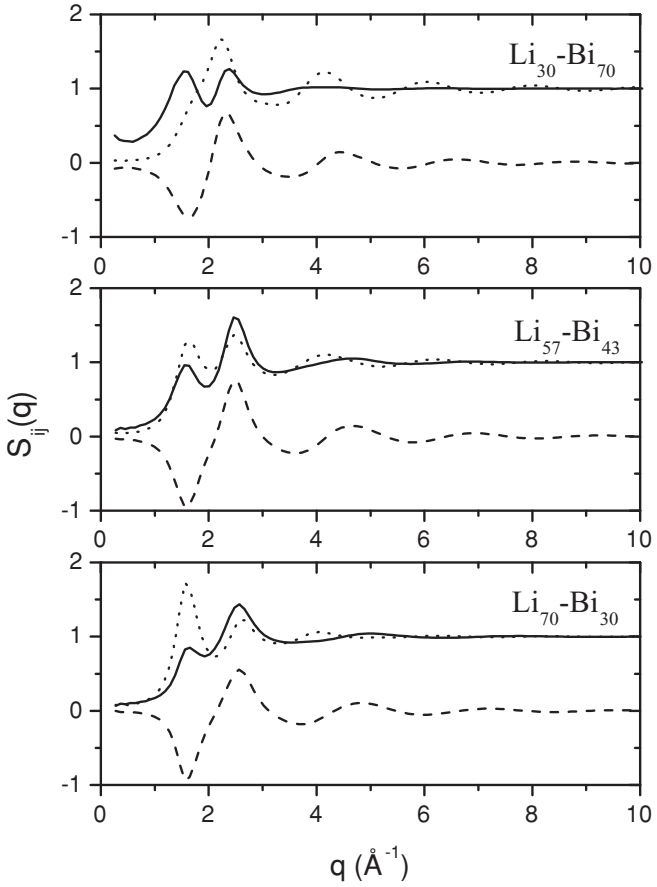

FIG. 8. Ashcroft-Langreth partial structure factors obtained from the classical simulations (Li-Li: solid; Li-Bi: dashed; Bi-Bi: dotted).

partial function between the minority species is lower than the second one. This could be understood in the following way; the atoms of the less numerous species tend to be surrounded by those of the other kind. So the first neighbor is most often of the other kind, which explains the shape of the curves. This feature is particularly pronounced in the case of Li_{70}-Bi_{30} and the above explanation is confirmed looking at a snapshot of the system (Fig. 7).

Looking at the partial Ashcroft-Langreth structure factors $S_{ij}(q)$ (Fig. 8), their usual large-q asymptotic limits are recovered. For each composition, the Li-Li function is unusual, presenting either a prepeak or two peaks with the same height. Considering their low-q limit, it should be noticed that the three partial functions tend to zero (except the Li-Li partial function in Li_{30}-Bi_{70}), a feature which is not observed in random mixtures like Na-K or K-Cs.

Using these partial functions, we computed the Bhatia-Thornton structure factors[22] which give insight into topological and chemical order (Fig. 9)

$$S_{\mathrm{nn}}(q) = c_1 S_{11}(q) + c_2 S_{22}(q) + 2\sqrt{c_1 c_2} S_{12}(q), \quad (6)$$

$$S_{\mathrm{nc}}(q) = c_1 c_2 \left[S_{11}(q) - S_{22}(q) + \frac{c_2 - c_1}{\sqrt{c_1 c_2}} S_{12}(q) \right], \quad (7)$$

$$S_{\mathrm{cc}}(q) = c_1 c_2 [c_2 S_{11}(q) + c_1 S_{22}(q) - 2\sqrt{c_1 c_2} S_{12}(q)]. \quad (8)$$

The topological functions $S_{\mathrm{nn}}(q)$ are very common, without any prepeak, low-q divergence, or shoulders of any kind. So, we do not observe any particular global topological feature. The lack of prepeak indicates that, at any composition, the alloys do not contain some permanent substructures like clusters or polyatomic ions. The coupling between topological and chemical order as depicted by $S_{\mathrm{nc}}(q)$ is also very common, looking like the corresponding function in liquid Na-K, for instance. But, considering $S_{\mathrm{cc}}(q)$, we have a clear indication of the heterocoodinated character of these mixtures. It unambiguously dips under the ideal mixture limit $c_{\mathrm{Li}} \cdot c_{\mathrm{Bi}}$ as q tends to zero. Extrapolating smoothly the curves to $q = 0$, we estimate the limits as 0.08, 0.019, and 0.011 ($\pm 10\%$) for Li_{30}-Bi_{70}, Li_{57}-Bi_{43}, and Li_{70}-Bi_{30}, respectively. This corroborates the picture we draw from the study of partial $g_{ij}(r)$. One more feature of $S_{\mathrm{cc}}(q)$ to be mentioned is the sharp first peak that indicates rather marked concentration fluctuations with a wavelength corresponding to twice the interatomic distance.

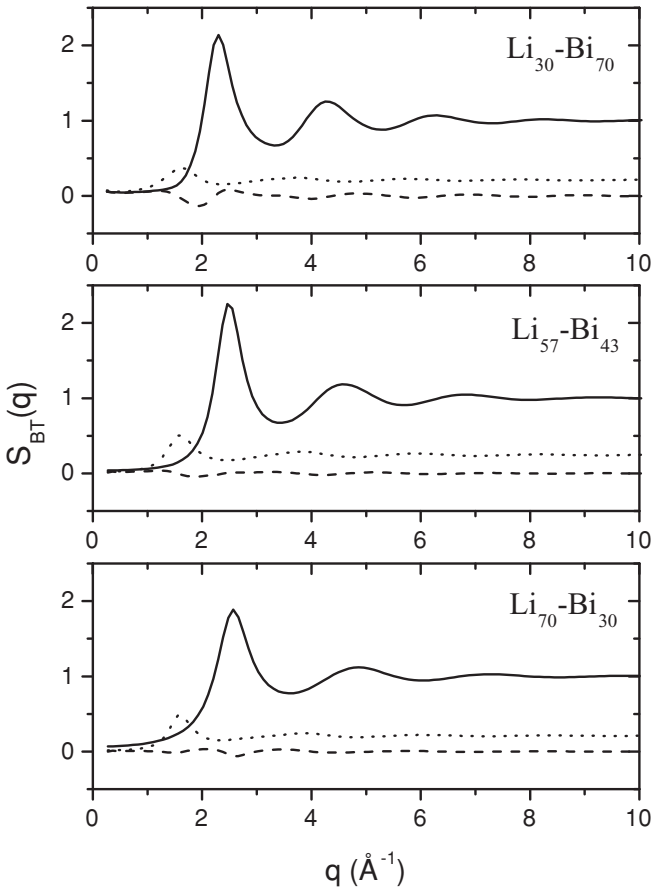

FIG. 9. Bathia-Thornton partial structure factors obtained from the classical simulations (S_{nn}: solid; S_{cc}: dotted; S_{nc}: dashed).

To better understand the atomic ordering in these mixtures, let us consider alloys of bismuth with alkali metals. Published structure data exist for K_{50}-Bi_{50} (Refs. 23,24), Rb_{50}-Bi_{50} (Ref. 24), Cs_{50}-Bi_{50}, and Cs_{75}-Bi_{25} (Ref. 25). In these three systems, experimental structure factors display prepeaks, which are attributed to the existence of Bi polyanions. Such a feature is not observed in our neutron structure factors, neither from simulation nor from experiments. However, this does not invalidate our results. Indeed, let A denote an alkali element. First, we recall that K-Bi, Rb-Bi, and Cs-Bi all display two congruent intermetallic compounds (A_3-Bi and A-Bi_2) as against only one (namely A_3-Bi) in the case of Li-Bi and Na-Bi. Second, considering the electronic transport properties of these five systems,[26,27] an evolution clearly occurs when going from Li- to Cs-Bi alloys. While the resistivity versus composition shows a single peak at A_{75}-Bi_{25} in the case of Li and Na alloys, a second one shows up at A_{60}-Bi_{40} in the case of K and Rb; this doublet moves to a single broad peak at the second composition in the case of Cs-Bi. This had been interpreted as follows: While the liquid phases of Li-Bi and Na-Bi display only the so-called A_{75}-Bi_{25} "octet compounds" in a given range of concentration, Cs-Bi liquid mixtures contain quite exclusively bismuth polyanions. As for K-Bi and Rb-Bi, they exhibit both features. The prepeaks were associated with the existence of the polyanions, which are absent in the case of Li and Na-Bi alloys and our results corroborate these assertions.

However, if stable Li_3-Bi "clusters" were to exist, there should appear a prepeak in the $S_{nn}(q)$ structure factor. Moreover, these clusters should be of trigonal planar kind, characterized by Li-Bi-Li angles equal to 120° and we would expect to see some effect on the coordination numbers. As already mentioned, we do not see any prepeak in the static structure factor, which means that there are no permanent structures on a scale larger than the interatomic distance. We also computed the coordination numbers which do not exhibit any significant behavior. Indeed, the total coordination number is above 11 whatever the composition and the kind of the central atom; such values are typical of random close packed structures. Looking also at the bond-angle distribution functions (not shown), we do not see any peak at 120°, especially in the partial Li-Bi-Li function. Thus, we believe that stable Li_3Bi entities do not exist in the liquid, but a strong heterocoordination is confirmed at every stage of our investigations.

Finally, our static structure results show that all three compositions considered in this study display a marked heterocoordination. This is all the more true when the composition gets closer to that of the intermetallic compound. Although permanent Li_3Bi clusters are not seen in this case, we cannot rule out the possibility that correlation between motion of atoms of different kinds exist. Therefore, it is interesting to consider now the diffusion properties.

D. Diffusion properties

Since these properties are highly sensitive to temperature, the results displayed now have been obtained at the same temperature for each composition, namely 1073 K, to be able to discuss the influence of the composition only. The self-diffusion coefficients have been computed from the velocity autocorrelation function (VACF)[28,29]

$$\psi(t) = \frac{1}{N} \lim_{\tau\to\infty} \frac{1}{\tau} \int_0^\tau \sum_{i=1}^{N} \mathbf{v}_i(t_0) \cdot \mathbf{v}_i(t_0 + t) dt_0, \qquad (9)$$

which also contains some information about the motion of the atoms. In this expression, $\mathbf{v}_i(t)$ denotes the velocity of the ith atom at time t. The functions are displayed in Fig. 10 for each component at each considered composition. In the same figure, we also display the spectral densities of these VACFs

$$\tilde{\psi}(\omega) = \int_{-\infty}^{+\infty} \psi(t) \exp(-i\omega t) dt. \qquad (10)$$

These curves merit several remarks. First, $\psi(t = 0) = 3k_BT/m$, explaining the ratio between the values in Li and Bi curves. The first minimum of the curves, when it exists, indicates the extent of the backscattering undergone by the particles. As can be seen, Li atoms, which are lighter, are more strongly backscattered than Bi ones. While a light particle will mostly be backscattered in a collision with heavier ones, a heavy atom will tend to break through a cage of light neighbors.

These arguments should also explain the evolution from the Bi-rich mixture to the Li-rich one. Indeed, in the first one, the

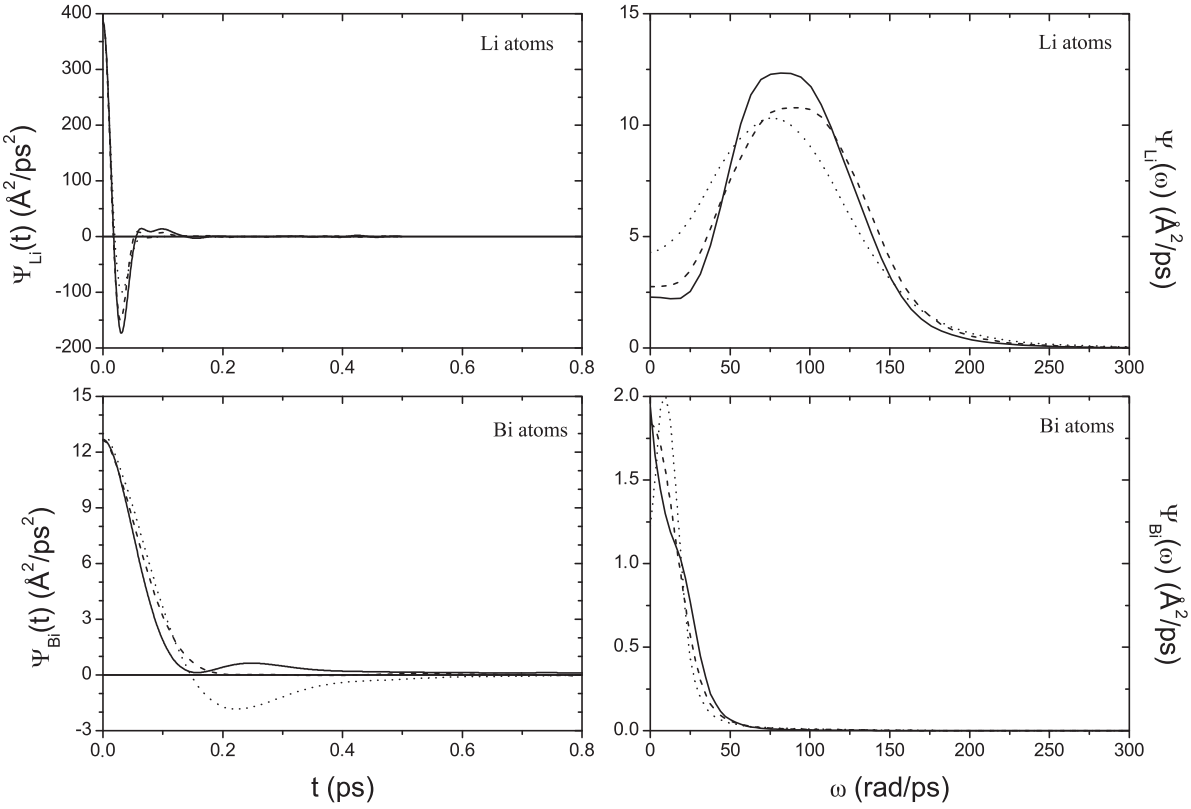

FIG. 10. Velocity autocorrelation function (left column) and corresponding spectral densities (right column) for lithium (top row) and bismuth atoms (bottom row) in Li_{30}-Bi_{70} (solid lines), Li_{57}-Bi_{43} (dashed lines), and Li_{70}-Bi_{30} (dotted lines) mixtures.

rebound should be amplified due to the presence of a larger proportion of heavy Bi atoms. This is observed with lithium, but the situation of bismuth is rather unexpected. Although one could have conjectured that Bi would diffuse more easily in Li-rich mixtures since the surrounding medium is less resistant, the opposite is observed. This might be correlated to the strong heterocoordination existing in this mixture. In agreement with the conclusions drawn on the structure of this melt since the diffusion of Bi atoms is hindered, we could imagine that Bi atoms do not diffuse alone, but with surrounding Li ones stuck on them. As we have already discussed, the bond is not stable and permanent; therefore we shall refer to this situation as Bi atoms loosely bound with some Li atoms. On one hand, this situation impedes bismuth atoms diffusion, and on the other hand, it improves that of Li which they transport, reducing their rebound.

Damped oscillations are also usually present in the long time tail of the VACF. When they exist, they are related to the oscillatory behavior of the atoms which are more or less confined in the cage of their surrounding neighbors (the so-called cage effect). When it exists, this oscillatory aspect of the individual motion of atoms is clearly recovered as a peak in the spectral density, the position of which corresponds to the collision frequency of the atoms. Of course, Li atoms, which are lighter, vibrate at a higher frequency than Bi atoms. For Li atoms, such a peak is clearly present in each case. Bi atoms display different behavior as a function of composition. The oscillations are clearly indicated as a peak or as a shoulder in the case of Li_{30}-Bi_{70} and Li_{70}-Bi_{30} alloys, while they nearly disappear in Li_{57}-Bi_{43}. Moreover, the vibrational feature is the more pronounced in the Li-rich mixture.

The motion of an atom in a liquid is also diffusive and this feature is recovered considering the low-frequency limit of the spectral density which is related to the self-diffusion coefficient as $D = \tilde{\psi}(\omega = 0)/6$. The fact that this limit is nonzero proves that the mixture is liquid and not solid. The estimated values of the coefficients are gathered in Table IV. Unsurprisingly, Li atoms diffuse more easily than Bi ones due to their lower mass. We also recover that the diffusion of Li atoms is easier in Li-rich environments than in Bi-rich ones, as well as the surprising, opposite evolution of the diffusion of Bi. It is important to recall that these results were obtained at the same temperature to avoid any temperature-related variations.

Finally, we have also computed the interdiffusion coefficient involved in Fick's law that describes the ability of both species to mix. This was obtained from the autocorrelation

TABLE IV. Self-diffusion and interdiffusion coefficients in the liquid alloys under consideration in Å^2/ps at 1073 K.

System	D_{Li}	D_{Bi}	$S_{cc}(0)$	$D_{Li/Bi}$	D_{id}	D_{Dark}
Li_{30}-Bi_{70}	0.381	0.323	0.08	0.727	0.364	0.954
Li_{57}-Bi_{43}	0.460	0.307	0.019	3.703	0.373	4.860
Li_{70}-Bi_{30}	0.716	0.204	0.011	7.598	0.358	6.834

function of the microscopic flux[2] not presented here

$$D_{\mathrm{Li/Bi}} = \frac{c_1 c_2}{S_{\mathrm{cc}}(0)} \int_0^\infty V_D(t)dt, \tag{11}$$

with

$$V_D(t) = \frac{1}{3Nc_1c_2} \lim_{\tau\to\infty} \frac{1}{\tau} \int_0^\tau \mathbf{v_d}(t_0)\cdot\mathbf{v_d}(t_0+t)dt_0, \tag{12}$$

where the microscopic diffusion velocity reads

$$\mathbf{v_d}(t) = c_2 \sum_{i=1}^{N_1} \mathbf{v}_i(t) - c_1 \sum_{j=1}^{N_2} \mathbf{v}_j(t). \tag{13}$$

The results are displayed in Table IV as well as the values obtained from the ideal mixture model ($D_{\mathrm{id}} = c_2D_1 + c_1D_2$) and from Darken's approximation [$D_{\mathrm{Dark}} = (c_2D_1 + c_1D_2)\cdot(c_1c_2)/S_{\mathrm{cc}}(0)$]. Whatever way it is computed (exact or Darken) the coefficient appears to be strongly composition dependent. The ideal mixture model is definitively ruled out, mainly due to the departure of $S_{\mathrm{cc}}(0)$ from its ideal mixture value $c_1 \cdot c_2$. Darken's approximation neglects the correlation between the velocities of particles of different species. Its predictions depart from the correct interdiffusion values by up to 30%. Moreover, a change in the sign of the difference is also noticeable when considering the Li-rich alloy. This means that the displacement of particles of different kinds are correlated and that a special diffusion regime characterizes this latter composition. This observation is consistent with the hypothesis we put forward according to which Li and Bi atoms could diffuse in loosely bound states. Anyway, the high values of $D_{\mathrm{Li/Bi}}$ indicate that both species mix easily and this is consistent with the strong heterocoordination observed in the structure.

IV. CONCLUSION

In this study, we have been interested in the structure and diffusion properties of Li-Bi alloys. These mixtures are more complex than nearly random ones and their description using classical simulations requires multiscale approaches rather than usual models of potential obtained from linear screening formalism.[1]

The methodology built up by Mihalkovič *et al*. has been successfully tested in the case of Li-Bi for three different compositions. We have reproduced the partial structures as obtained by *ab initio* methods and in agreement with the experiment. This double check allowed us to investigate in more detail the behavior of the mixtures, especially the chemical order and the diffusion properties.

LiBi is characterized by a strong chemical order correlated to a complex electronic structure. The conduction band is split into two subbands and a pseudogap exists at the Fermi level. The static structure reveals strong heterocoordination tendencies as confirmed by the very low values of $S_{\mathrm{cc}}(0)$. In the case of Li_{70}-Bi_{30}, this feature is related to a change in the nature of the chemical bond between atoms of different types. Its ionic nature increases, in agreement with the deepening of the pseudogap of the electronic structure and the expression of the corresponding pair potential. However, we did not find any sign of the existence of stable Li_3Bi compound, neither in the structure factors nor in the bond angle distribution.

Nevertheless, the study of the diffusion properties pointed out an anomalous evolution of the self-diffusion coefficient of bismuth as the lithium concentration is increased. Bismuth atoms are found to diffuse less easily in this composition range. This could be explained considering that bismuth and lithium atoms behave as if they were loosely bound, in agreement with the above-mentioned ionic nature of the interaction. The interdiffusion also shows that the mixture is not ideal at all and that both species have a strong propensity to mix.

The present study could not have been undertaken without a multiscale approach and this work opens several new perspectives. First, we have pointed out an anomaly in the diffusion properties, but it would be interesting to consider the dynamic structure factor since recently published experimental results have revealed the unique behavior of the collective excitations. Second, we have studied here a heterocoordinated mixture, but homocoordinated ones should also be considered, as well as alloys involving nonsimple metals, like transition metals, especially in view of their industrial applications. Validating the approach in these cases would open a wide scope of investigations.

ACKNOWLEDGMENTS

The PMMS (Pôle Messin de Modélisation et de Simulation) is greatly acknowledged for providing us with computer time. M.M. was supported by Grant No. VEGA 2/0111/11. F. Sacchetti is acknowledged for suggesting such a theoretical study on LiBi alloys.

[1] J. F. Wax and N. Jakse, Phys. Rev. B **75**, 024204 (2007).
[2] J. F. Wax, Physica B **403**, 4241 (2008).
[3] F. Ercolessi and J. B. Adams, Europhys. Lett. **26**, 583 (1994).
[4] M. Mihalkovič, C. L. Henley, M. Widom, and P. Ganesh, e-print arXiv:0802.2926v2.
[5] G. Kresse and J. Furthmüller, Comput. Mater. Sci. **6**, 15 (1996).
[6] G. Kresse and D. Joubert, Phys. Rev. B **59**, 1758 (1999).
[7] J. Sangster and A. D. Pelton, J. Phase Equilib. **12**, 447 (1991).
[8] S. V. Prokhorenko, Materials Science **32**, 482 (1996).
[9] L. E. Bove, F. Formisano, E. Guarini, A. Ivanov, C. Petrillo, and F. Sacchetti, Eur. Phys. Lett. **79**, 16002 (2007).
[10] G. Steinleitner, W. Freyland, and F. Hensel, Berichte der Bunsen-Gesellschaft für Physikallische Chemie, Bd. **79**, 1186 (1975).
[11] P. E. Blöchl, Phys. Rev. B **50**, 17953 (1994).
[12] P. Hohenberg and W. Kohn, Phys. Rev. **136**, B864 (1964).
[13] W. Kohn and L. J. Sham, Phys. Rev. **140**, A1133 (1965).
[14] J. P. Perdew, K. Burke, and M. Ernzerhof, Phys. Rev. Lett. **77**, 3865 (1996).
[15] J. P. Perdew, K. Burke, and M. Ernzerhof, Phys. Rev. Lett. **78**, 1396 (1997).
[16] P. Oelhafen, G. Indlekofer, and J. J. Güntherodt, Z. Phys. Chem. NF **157**, 483 (1988).
[17] J. Hafner and W. Jank, Phys. Rev. B **45**, 2739 (1992).

[18]L. E. Bove, F. Formisano, F. Sacchetti, C. Petrillo, A. Ivanov, B. Dorner, and F. Barocchi, Phys. Rev. B **71**, 014207 (2005).
[19]P. Heitjans, G. Kiese, C. van der Marel, H. Ackermann, B. Bader, P. Freiländer, and H. J. Stöckmann, Hyperfine Interact. **15–16**, 569 (1983).
[20]K. Hackstein, S. Sotier, and E. Lüscher, Journal de Physique (Colloques) **41**(C8), 49 (1980).
[21]N. W. Ashcroft and D. C. Langreth, Phys. Rev. **155**, 685 (1967).
[22]A. B. Bhatia and D. E. Thornton, Phys. Rev. B **2**, 3004 (1970).
[23]K. Hochgesand, R. Kurzhöfer, and R. Winter, Physica B **276–278**, 425 (2000).
[24]K. Hochgesand and R. Winter, J. Chem. Phys. **112**, 7551 (2000).
[25]S. A. van der Aart, V. W. Verhoeven, P. Verkerk, and W. van der Lugt, J. Chem. Phys. **112**, 857 (2000).
[26]J. A. Meijer and W. van der Lugt, J. Phys. Condens. Matter **1**, 9779 (1989).
[27]R. Xu, R. Kinderman, and W. van der Lugt, J. Phys. Condens. Matter **3**, 127 (1991).
[28]M. P. Allen and D. J. Tildesley, *Computer Simulation of Liquids* (Clarendon Press, Oxford, 1990).
[29]J. M. Haile, *Molecular Dynamics Simulation: Elementary Methods* (Wiley, New York, 1992).